

AQ:
#1

1 Polymer molded templates for nanostructured amorphous silicon 2 photovoltaics^{a)}

3 Lei Pei

4 *Department of Chemistry and Biochemistry, Brigham Young University, Provo, Utah 84602*

5 Amy Balls, Cary Tippetts, and Jonathan Abbott

6 *Department of Physics and Astronomy, Brigham Young University, Provo, Utah 84602*

7 Matthew Linford

8 *Department of Chemistry and Biochemistry, Brigham Young University, Provo, Utah 84602*

9 Jian Hu and Arun Madan

10 *MVSystems, Inc., Golden, Colorado 80401*

11 David Allred, Richard Vanfleet, and Robert Davis^{b)}

12 *Department of Physics and Astronomy, Brigham Young University, Provo, Utah 84602*

13 (Received 22 November 2010; accepted 20 January 2011)

AQ:
#2

14 Here, the authors report the fabrication of transparent polymer templates for nanostructured
15 amorphous silicon photovoltaics using low-cost nanoimprint lithography of polydimethylsiloxane.
16 The template contains a square two-dimensional array of high-aspect-ratio nanoholes (300 nm
17 diameter by 1 μm deep holes) on a $500 \times 500 \text{ nm}^2$ pitch. A 100 nm thick layer of *a*-Si:H was
18 deposited on the template surface resulting in a periodically nanostructured film. The optical
19 characterization of the nanopatterned film showed lower light transmission at 600–850 nm
20 wavelengths and lower light reflection at 400–650 nm wavelengths, resulting in 20% higher optical
21 absorbance at AM 1.5 spectral irradiance versus a nonpatterned film. © 2011 American Vacuum
22 Society. [DOI: 10.1116/1.3554720]

23 I. INTRODUCTION

24 Compared to crystalline silicon based solar cells, thin-film
25 hydrogenated amorphous silicon (*a*-Si:H) solar cells have the
26 potential advantages of less raw material usage and lower
27 fabrication costs as well as the benefits of high flexibility and
28 light weight. However, the efficiency of single-layer thin-
29 film *a*-Si:H solar cells is relatively low. Several efforts have
30 been made to increase single-layer cell efficiency by improv-
31 ing the light trapping of devices.

32 To achieve efficient light trapping researchers have devel-
33 oped a number of scattering techniques. These include ran-
34 domly textured substrates, such as Asahi-U type glass¹ and
35 other high-haze TCO material coatings² which scatter light at
36 their rough interfaces. The scattered light increases the effec-
37 tive optical path length for internally diffused light rays,
38 which widens the absorption window toward long light
39 wavelength. Metal nanoparticles^{3,4} have also been incorpo-
40 rated into photovoltaic systems as plasmonic structures for
41 light scattering and for exciting near-field charge carriers and
42 coupling light into guided modes. These techniques have
43 been applied either on the front or rear of the solar cell.^{5,6}
44 Periodically nanostructured plasmonic back contacts have
45 been reported to improve short-circuit current densities in the
46 spectral range from 550 to 800 nm. These demonstrated light
47 trapping, enhanced beyond that of a randomly textured cell.⁷
48 Another surface-texture geometry that has resulted in in-

creased efficiencies is the nanodome solar cell device with
significant higher absorption than flat solar cell.⁸ Subwave-
length gratings, which have consisted of a one-dimensional
array of lines with pitch smaller than the light wavelength,
have been used to suppress reflection over wide spectral
bandwidth and large field of view.^{9,10} In photovoltaic
applications,^{3,11–15} for example, periodically structured
ZnO:Al front contacts¹² have been implemented in amor-
phous silicon thin-film solar cells to reduce reflectance and
increase current density.

To directly measure light absorption in periodic nanopat-
terned *a*-Si:H films, we designed and fabricated a polymer
template with a square two-dimensional array of high-aspect-
ratio nanoholes (300 nm diameter by 1 μm deep holes) on a
 $500 \times 500 \text{ nm}^2$ pitch. A 100 nm thick layer of *a*-Si:H was
deposited on the template surface resulting in a periodically
nanostructured film and on planar surfaces for comparison.
Optical reflection and transmission measurements were then
conducted with an integrating sphere to capture both specu-
lar and scattered lights. In order to measure the effect of
nanoscale structuring on absorption of the amorphous silicon
without absorption contributions by other adjacent materials,
a simplified sample was fabricated without any metal back
reflector or electrode coating.

Besides the analysis of optical absorption, several other
aspects have been considered in this nanostructure design:
(1) the template can be cost-effectively incorporated into a
single junction thin-film PV device using conventional PV
film deposition techniques; (2) fast scalable production of the
template using roll-to-roll techniques¹⁶ can be applied on in-

^{a)}This paper was presented at the 57th Symposium of the American Vacuum Society.

^{b)}Electronic mail: davis@byu.edu

AQ:
#4

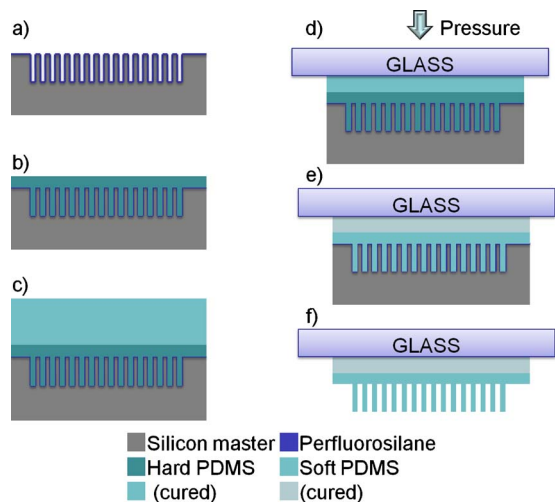


FIG. 1. (Color online) Scheme of nanoimprint process: (a) silicon master coated with perfluorosilane; (b) spin coating hard PDMS; (c) pouring soft PDMS on top of the hard PDMS; (d) placing a glass slide; (e) curing the PDMS stack; and (f) releasing the silicon master.

79 expensive polymer substrates; and (3) the patterned photo-
80 voltaic approach, when implemented at the appropriate di-
81 mensions, could have an impact on using PV materials
82 characterized by high defect densities including organic,
83 quantum dot, and oxide PV systems.

84 II. EXPERIMENT

85 The fabrication process for our three-dimensional nano-
86 structured polymer template has two main steps: silicon mas-
87 ter fabrication and nanoimprinting. A reusable silicon mas-
88 ter was first produced with a nanopillar array. This silicon mas-
89 ter was used as a mold to emboss on a polymer film via
90 nanoimprint lithography. This is a technique for high
91 throughput patterning of polymer nanostructures at great pre-
92 cision and at low costs.^{17,18} The process diagram is shown in
93 Fig. 1.

94 A. Electron-beam lithography

AQ: #5 95 ZEP 520A e-beam resist (Nippon Zeon) was spin coated
96 on a silicon wafer and baked on a hotplate at 170 °C for 2
97 min. ZEP has high sensitivity which is particularly valuable
98 for large area patterning and has relatively high plasma etch
99 resistance. To reduce resist charging during exposure, a layer
100 of conductive polymer was also spin coated on top of the
101 ZEP layer and baked on a hotplate at 90 °C for 30 s. The
102 designed pattern was a square about $5 \times 5 \text{ mm}^2$. This pattern
103 contains an 18×18 array of $300 \times 300 \text{ }\mu\text{m}^2$ squares with a
AQ: #6 104 $5 \text{ }\mu\text{m}$ overlap of the squares on each side. The $300 \text{ }\mu\text{m}$
105 squares are made of a series of perpendicularly crossed lines
106 with 500 nm pitch to form a grid pattern. An FEI/Philips
107 XL30 FEG ESEM (operating in high vacuum mode) with a
108 nanometer pattern generation system (JC Nability Lithography
109 Systems) was used for electron beam exposure. The electron
110 beam was set at 30 kV and the spot was set to size 5 (1172
111 pA) to allow fast writing. The magnification was $200\times$ and

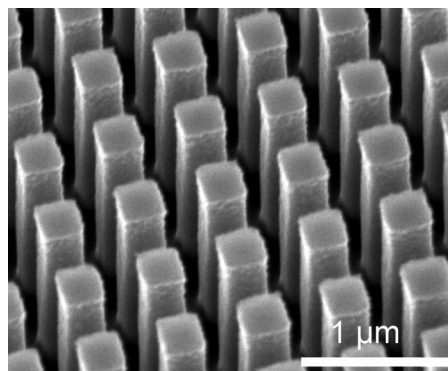


Fig. 2. SEM image of the patterned silicon wafer with nanopillar array.

the exposure line dose was 0.867 nC/cm. The exposed ZEP 112
sample was first rinsed with DI water to remove the conductive 113 AQ:
polymer, followed by development in ZED-N50 developer, 114 #7
rinsing in ZMD-D, and again rinsing in DI water. Finally, 115
the sample was put into an oxygen plasma etcher (Technics Planar-Etch II) 116
at 100 W for 1 min to descum the resist pattern. 117
118

B. Silicon master etching 119

The sample was then loaded into STS multiplex inductively 120
coupled plasma reactive ion etching with SF_6 and C_4F_8 121 AQ:
flow for directional etching. The exposed regions of the sili- 122 #8
con surface were etched down $1 \text{ }\mu\text{m}$. After etching, the 123
sample was put into the PE2 oxygen plasma etcher to re- 124
move most of the e-beam resist. The sample was then treated 125
in piranha solution to thoroughly clean and to add hydroxyl 126
groups on the surface. 127

C. Antiadhesion coating deposition 128

A perfluorosilane antiadhesion coating layer was deposited 129
on the surface of the silicon master via following steps. 130
The silicon master was put into a desiccator. A drop or two of 131
trichloro(1*H*, 1*H*, 2*H*, 2*H*-perfluorooctyl)silane (448931, 132
Sigma-Aldrich) were deposited in two scintillation vials 133
which were placed beside the master. The desiccator cham- 134
ber was pumped down with the laboratory vacuum for 10 135
min to accelerate the silane vaporization. Finally, the desic- 136
cator was sealed overnight to allow sufficient deposition on 137
the high-aspect-ratio pattern. This perfluorosilane antiad- 138
hesion coating had an advancing water contact angle over 118° , 139
which helps the silicon master separate from imprinted poly- 140
mer at the end of the nanoimprint process. Figure 2 shows 141
the resulting silicon nanopillar array master. 142

D. Nanoimprint patterning of the polymer 143

Polydimethylsiloxane (PDMS) was used for the patterned 144
polymer template. PDMS has the advantages of (1) low cost, 145
(2) optical transparency, and (3) thermal stability (well over 146
the temperature of 200 °C required for the silicon layer 147
deposition). Both hard PDMS and soft PDMS were employ- 148
ed in the process. The hard PDMS has a higher modulus 149

150 of elasticity and is used to replicate the high-resolution high-
 151 aspect-ratio template features. Soft PDMS was used as a glue
 152 to attach the hard PDMS to a glass slide.

153 To prepare hard PDMS, 3.4 g of a vinyl PDMS prepoly-
 154 mer (VDT-731, Gelest Corp.), 18 μL of a Pt catalyst (plati-
 155 num divinyltetramethyldisiloxane, SIP6831.1, Gelest Corp.),
 156 and one drop of a modulator (2,4,6,8-tetramethyl-
 157 tetravinylcyclotetrasiloxane, 87927, Sigma-Aldrich) were
 158 mixed and degassed for 15 min in a vacuum desiccator. 1 g
 159 of a hydrosilane prepolymer (HMS-301, Gelest Corp.) was
 160 then gently stirred into this mixture and degassed for another
 161 2 min. Immediately (within 3 min), this hard PDMS mixture
 162 was spin coated onto the silicon master at 1000 rpm for 40 s,
 163 forming a 30–40 μm thick layer. Hard PDMS thus fully
 164 covered the nanopillars on the silicon master. The coated
 165 master was then put into an oven and partially cured for 30
 166 min at 60 $^{\circ}\text{C}$.

167 The soft PDMS prepolymer Sylgard 184 PDMS (Dow
 168 Corning) base and curing agent were mixed 10:1 and de-
 169 gassed for 30 min ahead of time. This liquid prepolymer was
 170 poured onto the hard PDMS layer immediately after the par-
 171 tial curing, while the hard PDMS was still slightly tacky. The
 172 partially completed structure was then degassed in a vacuum
 173 desiccator for 1 h. After a glass slide was placed on the soft
 174 PDMS and a 530 g weight was placed on the glass slide (Fig.
 175 1), the structure was returned to the vacuum for further de-
 176 gassing to remove any bubbles between the soft PDMS and
 177 the glass. The PDMS stack was slowly cured at room tem-
 178 perature (overnight, 12–14 h). Fast curing at high tempera-
 179 ture can cause the hard PDMS to crack. After this slow cur-
 180 ing, the entire assembly was placed in an oven at 60 $^{\circ}\text{C}$ for
 181 a 1 h hard bake. The composite PDMS template was then
 182 released from the master surface by carefully peeling the
 183 template from the surface while they were still warm. Figure
 184 3 shows the optical and scanning electron microscopy (SEM)
 185 images of the imprinted nanoholes, which are the inverse of
 186 the silicon master pattern.

187 E. Photovoltaic material deposition

188 Patterned and unpatterned PDMS layer regions on a glass
 189 slide were simultaneously coated with 100 nm amorphous
 190 silicon by plasma enhanced chemical vapor deposition
 191 (PECVD). The deposition was done in an MVSystems
 192 PECVD reactor (MVSystems, Inc.) at 200 $^{\circ}\text{C}$ from pure si-
 193 lane gas. The amorphous silicon produced in this study re-
 194 sults in a typical hydrogen concentration of $\sim 10\%$; the op-
 195 tical bandgap is of 1.7–1.8 eV. For planar amorphous silicon
 196 layers of 100 nm thickness, the largest gain in absorption
 197 in the wavelength range of 400–540 nm as the absorption
 198 coefficient of the material becomes $>1 \times 10^5/\text{cm}$ in this
 199 wavelength range. For sample description, the area outside
 200 the nanostructured region is labeled “planar” sample, while
 201 the area inside nanostructured template is labeled as a “pat-
 202 terned” sample; both samples consisted of a
 203 glass/PDMS/*a*-Si:H stack. The 100 nm layer thickness was
 204 chosen because in amorphous silicon devices the Staebler–
 205 Wronski degradation limits the active layer thickness for

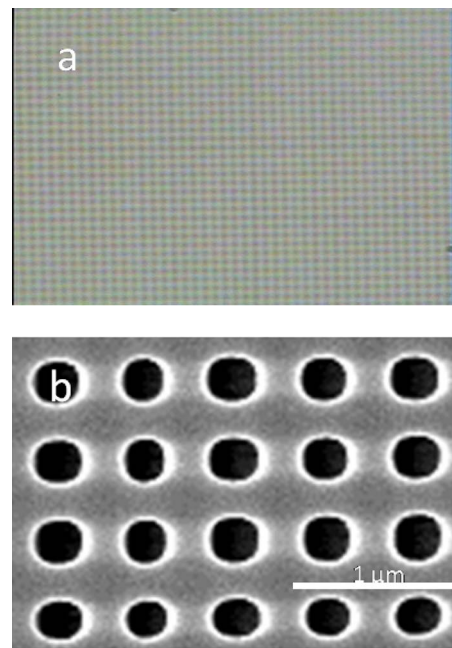


FIG. 3. (Color online) (a) Optical and (b) SEM images of embossed nanoholes.

highly efficient carrier extraction to approximately 100 nm.¹⁹ 206
 At this thickness, however, planar layers capture little of the 207
 light at wavelengths above 600 nm. Figure 4(a) shows a 208
 SEM front view of the patterned sample. The diameter of the 209
 nanoholes was reduced by around 100 nm on the surface by 210
 the amorphous silicon deposition. In the cross-section image 211
 [Fig. 4(b)] processed by focused ion beam (FIB), 100 nm of 212
 amorphous silicon (which shows up as black) can be seen 213
 deposited mostly at the top of the posts with the coating 214
 continuing down the posts approximately 150 nm. 215

F. Optical measurement setup

216
 Reflectance and transmission as a function of wavelength 217
 were measured on both patterned and planar samples. A 218
 tungsten lamp was used as the light source. The light beam 219
 was collimated with a lens tube. Then the light passed 220
 through an aperture to reduce the beam diameter to approxi- 221
 mately 3 mm, which is small enough to easily align with the 222
 $5 \times 5 \text{ mm}^2$ nanopatterned area. A 2 in. diameter integrating 223
 sphere with a 99% reflectance coating (Thorlabs, IS236A-4) 224

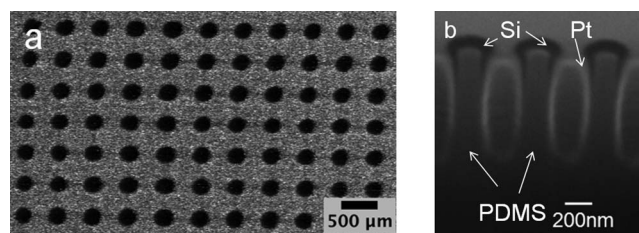


FIG. 4. (a) SEM top view of *a*-Si coated patterned polymer template; (b) cross-section view presents Pt (FIB deposited), *a*-Si (dark cap), and PDMS post, starting from the top and moving down a post.

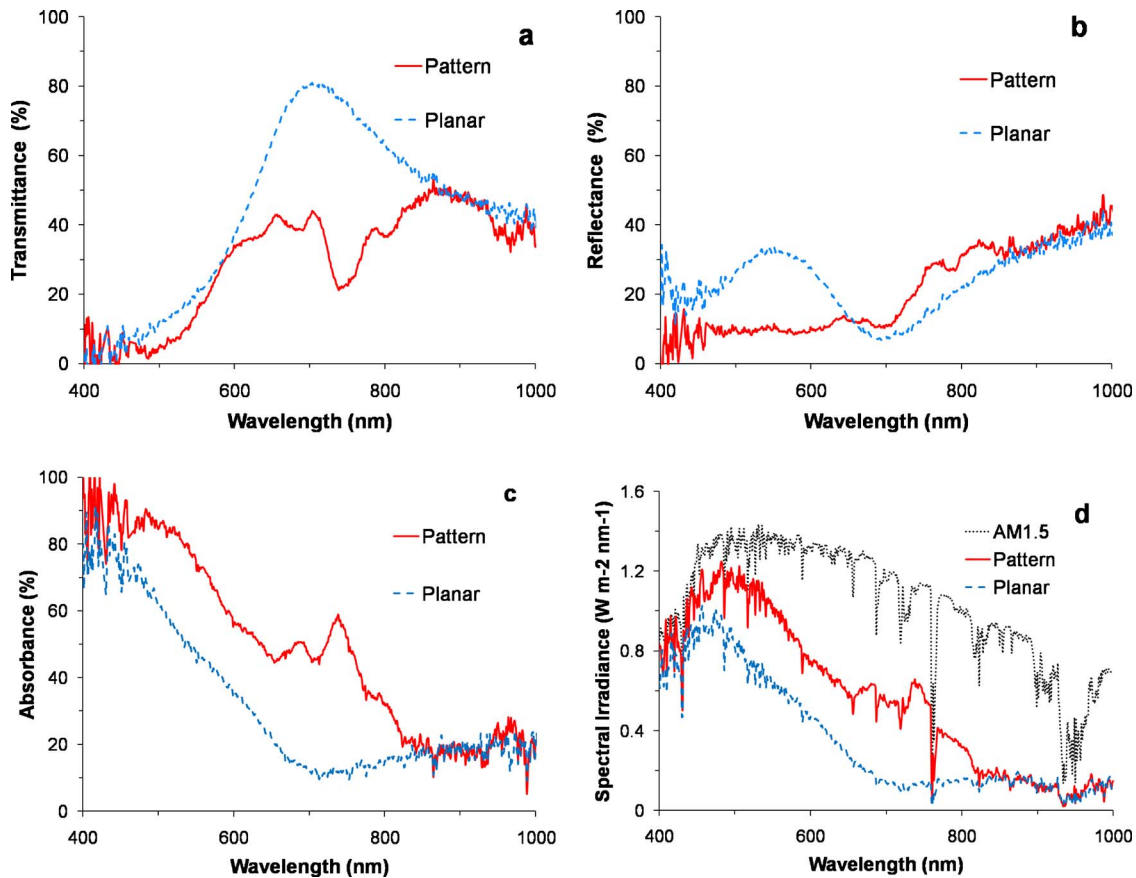


FIG. 5. (Color online) (a) Transmittance spectra of patterned and planar areas; (b) reflectance spectra of patterned and planar areas; (c) absorbance spectra of patterned and planar areas; and (d) spectral irradiance of AM 1.5 and weighted absorbance of patterned and planar areas.

225 was used for transmission, reflection, and incident beam intensity measurements. A Czerny–Turner charge-coupled device (CCD) spectrometer (Science-Surplus, compact fiber 227 coupled CCD spectrometer, 365–1100 nm) was fiber coupled 228 to the detector port of the integrating sphere. 229

230 For the total beam intensity measurements, the entrance 231 port of the integrating sphere was opened but the sample port 232 at 180° was closed. The incident beam passed through the 233 center of the entrance port striking the diffuse white reflective 234 surface on the sample port scattering evenly around the 235 sphere. The obtained spectrum was used as the “total” beam 236 intensity to compare with the transmission and reflection 237 spectra. For transmission measurements the sample was 238 placed perpendicular to the incident beam in front of the 239 entrance port. For reflection measurements the 180° port of 240 the integrating sphere (opposite the entrance port) was 241 opened and the sample, tilted at a 5° angle relative to the 242 perpendicular, was placed up against this port. The tilt on the 243 sample insures that light reflected specularly from the sample 244 hits the side of the integrating sphere. Without it specular 245 light could leave through the entrance port and not reach the 246 detector.

247 III. OPTICAL RESULTS AND DISCUSSION

248 The transmittance (relative to total beam) spectra [Fig. 249 5(a)] show a significant difference between patterned and

250 planar samples at longer wavelengths (600–850 nm). Especially 251 around 700–750 nm, the patterned sample transmits 252 40%–50% less light than the planar sample. Lower light 253 reflection of the patterned sample was also observed at 400– 254 650 nm wavelengths [Fig. 5(b)]. There are many sharper 255 optical features seen between 600 and 800 nm; we attribute 256 these features to complex optical resonances of our subwave- 257 length periodic structures.

258 The absorbance spectra [Fig. 5(c)] were calculated from 259 transmittance and reflectance spectra. The spectra show that 260 the patterned area has higher absorption in most of the visible 261 spectrum. At longer wavelengths (650–800 nm), where the 262 absorption of the planar area is very low, the patterned 263 area has significantly more absorption.

264 The weighted absorbance spectra [Fig. 5(d)] were calculated 265 from the absorbance spectra weighted by the spectral 266 irradiance AM 1.5 spectra. The integrated weighted absor- 267 bance for patterned and planar samples shows that the patterned 268 sample captured 55% of spectral irradiance energy, while the 269 planar sample only got 35%. Moreover, this 20% 270 improvement might be further increased by optimizing the 271 amorphous silicon deposition profile.

272 Experimentally it is possible that in transmission (reflection) 273 measurements light scattered (reflected) at wide angles 274 ($>70^\circ$ relative to the normal) will not enter into and be 275 collected in the integrating sphere due to a $\pm 70^\circ$ acceptance

276 angle of the sphere ports. Such light could appear as an in-
 277 crease in absorption. Also, there is drift in the light source as
 278 well as detector noise that will result in some uncertainty in
 279 the absorption measurement. By measuring reflection and
 280 transmission on patterned and unpatterned transparent
 281 PDMS only samples, we were able to put an upper bound on
 282 the uncertainty of the absorption measurement due to sys-
 283 tematic factors such as noncollected light. There is some
 284 wide-angle low-intensity scattering ($>70^\circ$ from normal)
 285 from the patterned PDMS sample; however, reflection and
 286 transmission measurements account for all of the incident
 287 light with less than 5% uncertainty. There is similar wide-
 288 angle scattering from the *a*-Si:H coated template but it is
 289 much dimmer than from the transparent PDMS sample; it
 290 should therefore result in measurement uncertainties less
 291 than 5% of incident.

292 The increased absorption at longer wavelengths is not due
 293 to lower reflection; that is, the effect is not simply antireflec-
 294 tion. In fact, at longer wavelengths (600–800 nm) the reflec-
 295 tion of patterned samples is slightly higher than the reflection
 296 of planar samples. Nevertheless, at these long wavelengths
 297 the patterned sample absorption is much higher. Since the
 298 only absorbing material in the sample is amorphous silicon,
 299 this difference results from increased absorption in the sili-
 300 con. Since there is the same amount of silicon per area as the
 301 planar sample, the effective light path through the silicon
 302 must be longer. This is consistent with coupling of the light
 303 into in-plane guided modes as proposed by other researchers
 304 at grating periods on this scale.^{7,14} However, in prior work,
 305 direct measurement of absorption by the semiconductor has
 306 not been possible due to the presence of nanopatterned metal
 307 layers. Our results here indicate that the nanopatterned semi-
 308 conductor itself acts as an effective coupling grating.

309 Periodic patterning can also minimize reflection, as we
 310 see at the short wavelength end of the spectrum in Fig. 5(b).
 311 Eisele *et al.*¹² showed that periodic patterning reduced reflec-
 312 tions most effectively at 980 nm pitch. However, a shorter
 313 pitch is likely required for maximum coupling of the light
 314 into guided modes. Our absorption work indicates that with a
 315 500 nm pitch we are effectively coupling 600–800 nm light,
 316 increasing absorption at the wavelengths most critical for
 317 light capture in amorphous silicon. Light capture is critical at
 318 the long wavelength end of the visible spectrum because *a*-Si
 319 has such a very small absorption coefficient there. This is
 320 also in contrast to random textures that increase absorption
 321 nonresonantly resulting in a smaller absorption gain where it
 322 is most needed.⁷

IV. CONCLUSION

We have developed a low-cost-template fabrication pro-
 cess for nanostructuring of amorphous silicon into a layer
 with a two-dimensional array of holes. This geometry was a
 convenient platform for optical absorption measurements on
 nanopatterned semiconductor layers. The increased absorp-
 tion in the nanohole array indicates coupling to lateral guided
 surface modes. This approach provides a test bed for absorp-
 tion studies in nanostructured film geometries and should
 result in improved light capturing designs in thin-film solar
 cells.

ACKNOWLEDGMENTS

The authors acknowledge the support of CHIRP Grant
 from the College of Physical and Mathematical Sciences at
 Brigham Young University. One of the authors (C.T.) was
 supported by a grant from the BYU Office of Research and
 Creative Activities. The authors thank Steven Schultz of the
 BYU Department of Electrical Engineering for useful discus-
 sions.

- ¹K. Sato, Y. Gotoh, Y. Wakayama, Y. Hayasahi, K. Adachi, and H. Nishimura, Rep. Res. Lab. Asahi Glass Co. Ltd. **42**, 129 (1992). 342
- ²J. Krč, F. Smole, and M. Topič, Prog. Photovoltaics **11**, 429 (2003). 344
- ³H. A. Atwater and A. Polman, Nature Mater. **9**, 205 (2010). 345
- ⁴K. Nakayama, K. Tanabe, and H. A. Atwater, Appl. Phys. Lett. **93**, 121904 (2008). 346
- ⁵R. H. Franken, R. L. Stolk, H. Li, C. H. M. van der Werf, J. K. Rath, and R. E. I. Schropp, J. Appl. Phys. **102**, 014503 (2007). 348
- ⁶S. Fahr, C. Rockstuhl, and F. Lederer, Appl. Phys. Lett. **92**, 171114 (2008). 350
- ⁷V. E. Ferry, M. A. Verschuuren, H. B. T. Li, E. Verhagen, R. J. Walters, R. E. I. Schropp, H. A. Atwater, and A. Polman, Opt. Express **18**, A237 (2010). 352
- ⁸J. Zhu, C. M. Hsu, Z. F. Yu, S. H. Fan, and Y. Cui, Nano Lett. **10**, 1979 (2010). 355
- ⁹Y. Kanamori, E. Roy, and Y. Chen, Microelectron. Eng. **78–79**, 287 (2005). 357
- ¹⁰Y. Kanamori, K. Kobayashi, H. Yugami, and K. Hane, Jpn. J. Appl. Phys., Part 1 **42**, 4020 (2003). 358
- ¹¹N. Senoussaoui, M. Krause, J. Muller, E. Bunte, I. Brammer, and H. Stiebig, Thin Solid Films **451–452**, 397 (2004). 361
- ¹²C. Eisele, C. E. Nebel, and M. Stutzmann, J. Appl. Phys. **89**, 7722 (2001). 362
- ¹³K. Sopian, N. Asim, N. Amin, and S. H. Zaidi, European Journal of Scientific Research **24**, 358 (2008). 363
- ¹⁴K. Söderström, F. J. Haug, J. Escarré, O. Cubero, and C. Ballif, Appl. Phys. Lett. **96**, 213508 (2010). 364
- ¹⁵C. Haase and H. Stiebig, Prog. Photovoltaics **14**, 629 (2006). 365
- ¹⁶R. E. I. Schropp and M. Zeman, IEEE Trans. Electron Devices **46**, 2086 (1999). 366
- ¹⁷L. J. Guo, Adv. Mater. (Weinheim, Ger.) **19**, 495 (2007). 367
- ¹⁸T. W. Odom, J. C. Love, D. B. Wolfe, K. E. Paul, and G. M. Whitesides, Langmuir **18**, 5314 (2002). 368
- ¹⁹A. Luque and S. Hegedus, *Novel (Firm), Handbook of Photovoltaic Science and Engineering* (Wiley, Hoboken, NJ, 2003), p. 1138. 369

AUTHOR QUERIES — 311102JVA

- #1 Au: Please supply place and date in title note.
- #2 Au: Please verify insertion of squared in 500x500 nm throughout.
- #3 Au: Please spell out TCO.
- #4 Au: Please supply definition of PV.
- #5 Au: Please supply definition of ZEP.
- #6 Au: Please check insertion of squared after micron.
- #7 Au: Please supply definition of DI.
- #8 Au: Please spell out STS.